arXiv:1402.3133v1 [physics.acc-ph] 13 Feb 2014

Unveiling the orbital angular momentum and acceleration of electron beams

Roy Shiloh,[1,*] Yuval Tsur,[1] Yossi Lereah,[1] Boris A. Malomed,[1] Vladlen Shvedov,[2] Cyril Hnatovsky,[2] Wieslaw Krolikowski,[2] and Ady Arie[1]

[1]*Department of Physical Electronics, Fleischman Faculty of Engineering, Tel Aviv University, Tel Aviv 6997801, Israel*
[2]*Laser Physics Centre, The Australian National University, Canberra ACT 0200, Australia*

New forms of electron beams have been intensively investigated recently, including vortex beams carrying orbital angular momentum, as well as Airy beams propagating along a parabolic trajectory. Their traits may be harnessed for applications in materials science, electron microscopy and interferometry, and so it is important to measure their properties with ease. Here we show how one may immediately quantify these beams' parameters without need for additional fabrication or non-standard microscopic tools. Our experimental results are backed by numerical simulations and analytic derivation.

PACS numbers:

In the last few years it became possible to generate special shapes of electron beams. One of these special beams is the vortex beam [1–3] having a helical wavefront structure and a phase singularity on axis. Its azimuthal phase dependence is $\exp(il\phi)$, where integer l is the topological charge and ϕ is the azimuthal angle. This beam carries an orbital angular momentum of $\hbar l$ [4]. Another interesting beam is the Airy beam, having a transverse amplitude dependence in the form of the Airy function, i.e. $\mathrm{Ai}(x/x_0)$, where x_0 defines the transverse scale. It is shape-preserving and moves along a parabolic trajectory in free-space with a nodal trajectory coefficient, sometimes referred to as the "acceleration" coefficient, $1/2x_0^3k^2$, where k is the wave number. These beams, generated and observed in a TEM (Transmission Electron Microscope) are expected to open new possibilities for interactions between electrons and matter, as well as for electron microscopy and interferometry. For example, vortex beams were used in electron energy loss spectroscopy in order to characterize the magnetic state of a ferromagnetic material [1], while Airy beams were proposed for realization of a new type of electron interferometer [5]. In order to utilize these new types of electron beams, it is required to develop methods that allow one to easily determine their defining properties - the OAM in the case of a vortex beam or the nodal trajectory coefficient in the case of an Airy beam.

Recently, a new method was proposed for measuring the OAM of electron beams [6] in TEM. Two holographic plates were used: a vortex-generating spiral plate in the condenser aperture and a fork grating acting as an analyzer in the selected-area aperture. This method relies on a custom modification of the objective aperture, which requires technical specialists and is less desired in routinely-operated facilities, though it is advantageous for mixed-state OAM-carrying modes. In this Letter, we demonstrate a straightforward method for OAM pure-state determination, which dispenses with fabrication or aperture-manipulation. We then extend the idea to the measurement of the nodal trajectory of electron Airy beams, along with supporting simulations and mathematical derivation.

In their 1991 article [7] Abramochkin and Volostnikov discussed the mathematics of beam transformations under astigmatic conditions. Since then, different authors proposed and demonstrated mode conversion in lasers [8], linear and nonlinear optics [9, 10] and free-electron beams in TEM [11]. In the latter work, Schattschneider et. al. have shown in theory and experiment how first-order Laguerre-Gauss modes may be transformed to first-order Hermite-Gauss modes. Recently, it was proposed that a cylindrical lens acting as a mode converter [12] be used to quantify the OAM of optical vortices [13]. Thus, a vortex of integer topological charge converts into a corresponding Hermite-Gauss-like mode, where the number of dark stripes precisely indicates the topological charge. The method's advantage is in its simplicity and generality: the only addition to the setup is a cylindrical lens. In the TEM, the lens is inherent - the condenser and objective stigmators may be used to impose a strong astigmatism along a desired axis, thereby implementing the elliptic transformation required to perform mode conversion.

Other OAM-measuring methods have previously been investigated [14], some examples of which include interaction with additional holographic plates [15], performing a geometric optical transformation [16], modal decomposition [17] and optical transformations [18].

In our experiment, we designed a two-dimensional binary hologram - a fork grating which is mathematically written

$$h(x,y) = \mathrm{sign}\left\{\sin\left[\frac{2\pi x}{\Lambda} - l\cdot\mathrm{atan2}(y,x) + \delta\frac{\pi}{2}\right] + \Delta\right\} \quad (1)$$

where $2\pi x/\Lambda$ is a linear grating along x, with period Λ, upon which the four-quadrant inverse-tangent function[27] modulates the spiral phase of the vortex, l being the topological charge. δ reduces fabrication errors in the centre by preserving continuity: thus its value is chosen equal to zero (one) if l is odd (even). Δ relates to duty cycle; we chose $\Delta = 0.25$ so both even and odd diffraction orders are visible. A Raith Ion-Line focused ion-beam (FIB) was used to mill into a 100 nm SiN membrane coated by 50 nm Au, from the gold side. The function of the gold layer is two-fold: to prevent charging of the sample and to assure the membrane behaves as an amplitude (binary) grating.

A fork grating with $l = 3$ topological charge was fabricated (Fig. 1e), based on a $\Lambda = 0.750\,\mu$m period, along with a linear (Bragg) grating of period $\Lambda = 0.445\,\mu$m which was fabricated for calibration purposes (Fig. 1f). The sample was mounted onto a Tecnai F-20 FEG-TEM with a single tilt specimen holder, and subsequently observed in the microscope in Low Angle Diffraction (LAD) mode through a $10\,\mu$m aperture.

In order to form the far field diffraction pattern, the condenser lens was set so a focused spot is measured. The fork grating was then aligned under the beam and the hologram imposed a spiral phase such that in each diffraction order m, a vortex of OAM $l \cdot m$ emerged (Fig. 1a). The intense on-axis (zero-order) beam was blocked to prevent damage to the CCD.

Since the electron beam impinging on the hologram does not have a Gaussian distribution, the emerging vortices are not strictly Laguerre-Gauss modes. However, the resulting diffraction pattern is undeniably dominated by solutions of the Schrödinger equation

$$\left[\nabla_{\perp}^2 + 2ik_{DB}\frac{\partial}{\partial z}\right]\psi = 0 \tag{2}$$

where $k_{DB} = 1/\lambda_{DB}$ is the de-Broglie wave-number. This equation governs the paraxial dynamics of the slowly varying envelope of the free electron beam in the TEM[19], a statement which is augmented by the results of the next step in our experiment.

The electron beam is made sufficiently astigmatic along the desired axis so it becomes elliptic; in the present case, this axis must be parallel to the lateral direction of the fork. As a reference, the linear grating was first measured under these conditions. As will be explained below, we purposely measured slightly out of the focal plane (Fig. 1c). This reference serves to assess the power of the astigmatism, or, the efficacy of the elliptic transformation. When the beam is sufficiently elliptic, the vortices in the different diffraction orders are converted into Hermite-Gauss-like modes (Fig. 1b) and the resulting dark stripes indicate the OAM carried by each order. In addition, the angle of the transformed orders signifies the rotation direction of the vortex: clockwise or counter-clockwise. The linear grating's diffraction spots become lines, as expected from a cylindrical lens (Fig. 1d). Note that if the linear grating's diffraction pattern was observed in focus rather than out of it, the spots would be so small that the equipped Gatan 694 CCD would not be able to distinguish the ellipticity of the beam; also, the additional diffraction lines visible in the negative orders (Fig. 1d) are a result of asymmetry of the sample relative to the beam, introduced by using a single-tilt rather than a double-tilt holder. In the supplementary material, we show a similar, additional measurement of at least $10\hbar$.

We then used the same principle to investigate the acceleration of 2D Airy beams. Optical generation and manipulation of Airy beams [20, 21] has been recently under the spot-light; here we present, to the best of our knowledge, the first encounter of Airy beams with special transformations, specifically the astigmatic transformation.

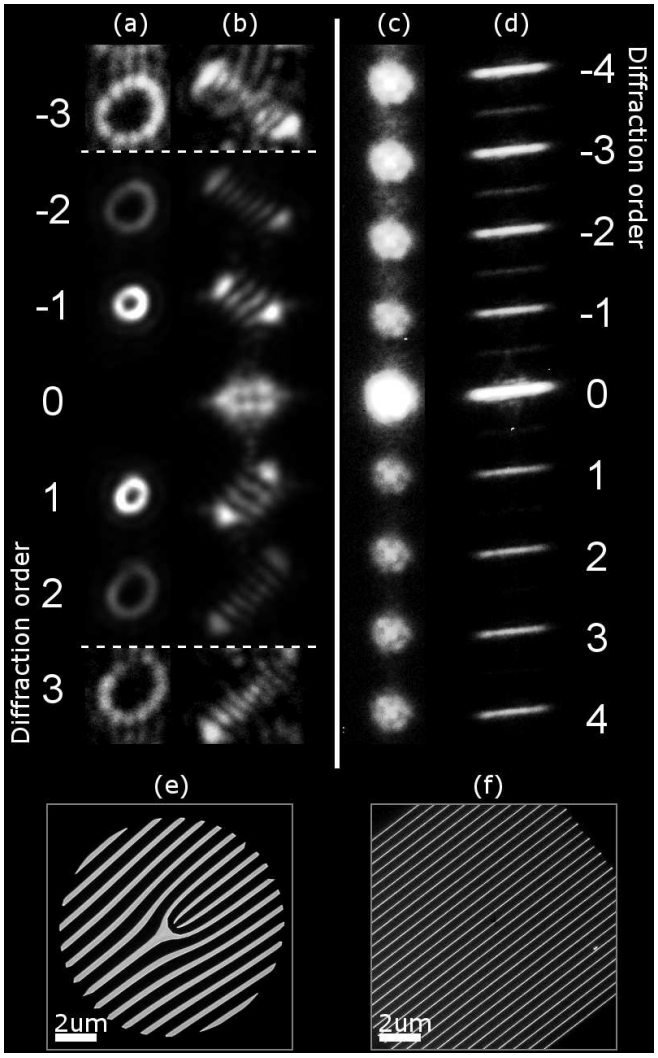

Figure 1: (Color online) Experimental results: diffraction patterns of (a) vortices generated by a charge 3 fork grating, using a focused stigmatic beam (zero-order blocked); (b) corresponding vortices after elliptic transformation; (c) diffraction pattern generated by a linear calibration grating using a stigmatic beam, out of focus; (d) corresponding lines resulting from the elliptic transformation, out of focus. Below: TEM images of (e) charge 3 fork ($0.750\,\mu$m period); (f) linear grating ($0.445\,\mu$m period). Note: brightness levels in the third order parts, as marked by the dashed lines in (a) and (b), have been modified for visibility.

For the purpose of generality, we express the transformation of a beam, $f(\xi,\eta)$, under general astigmatic conditions by

$$F\left(k_\xi, k_\eta, a\right) = \int_{-\infty}^{\infty}\int_{-\infty}^{\infty} e^{i\left(k_\xi \xi + k_\eta \eta\right) + i\psi(\xi,\eta,a,\alpha)} f(\xi,\eta)\, d\xi\, d\eta. \tag{3}$$

Here we define the Cartesian coordinates (ξ,η) in the plane of the holographic mask, and similarly $\left(k_\xi, k_\eta\right)$ in the diffraction plane. $\psi(\xi,\eta,a,\alpha) = a\left[\left(\xi^2-\eta^2\right)\cos 2\alpha + 2\xi\eta\sin 2\alpha\right]$

and a,α are defined as in [7]. In that paper, it is shown that in the special case of $\psi(\xi,\eta,a,\alpha=\pi/4)=2a\xi\eta$, Hermite-Gauss and Laguerre-Gauss beams interchange; this mathematical paradigm explains our previous results.

Applying the transformation to Airy beams, one may generally write

$$F\left(k_\xi,k_\eta,a\right)=\int_{-\infty}^{\infty}\int_{-\infty}^{\infty}e^{i\left(k_\xi\xi+k_\eta\eta\right)+2ai\xi\eta}e^{i\left(\xi^3+\eta^3\right)/3\widetilde{\beta}^3}d\xi d\eta, \tag{4}$$

where $\widetilde{\beta}$ relates to the beam's nodal trajectory (sometimes referred to as "acceleration" coefficient, through $\widetilde{\beta}^3/2$). In a diffractive system with focal length f, we define

$$\mathfrak{a}=\beta^3 k_{\mathrm{DB}}/2f^3, \tag{5}$$

where β is defined below through fabrication parameters and k_{DB} is the de-Broglie wavelength. While calculation of this integral in the stigmatic ($a=0$) case is easy and results in the two-dimensional Airy pattern, obtaining a closed-form analytic solution to the astigmatic ($a\neq 0$) case is difficult. In order to measure the nodal trajectory coefficient from a stigmatic pattern, one must either record the propagation of the Airy beam in different planes and measure the actual trajectory, or directly measure the density of the Airy lobes and relate it to the length scale x_0 (for more details, see [5]). These two methods are, unfortunately, time consuming and arduous; the latter case, for example, is generally dangerous to perform experimentally, since such a measurement requires the pattern to be in focus, to exhibit high-contrast and low signal-to-noise ratio so as to make the lobes discernible and measurable with precision, all the while protecting the CCD camera from damage. Using astigmatic transformation, we show that the intensity of the beam is distributed over a large area and the beam's acceleration coefficient is deduced from the asymptotic angle (as defined by a hyperbolic curve in elliptic coordinates).

In our experiment, we designed $30\mu m$-diameter binary masks using the expression

$$h(\xi,\eta)=\mathrm{sign}\left\{\cos\left[\left(\xi^3+\eta^3\right)/3\beta^3\right]\right\} \tag{6}$$

where β^3 determines the amount of cubic phase, thereby controlling the generated Airy's nodal trajectory. A large ensemble of these β-varying astigmatic Airy beams were simulated, and in the resulting elliptic coordinate-system, we naturally fitted hyperbolae to these curves, see Fig. 2. Hyperbolae may be represented in the positive x half-space of a Cartesian coordinate system by using the following relations:

$$\begin{aligned}x&=b\cosh(u)\cos(v)\\ y&=\pm b\sinh(u)\sin(v)\end{aligned} \tag{7}$$

where b is a real positive constant, $u\in[0,\infty)$ is the curved coordinate along the hyperbola and $v\in[0,\pi/2)$ is the asymptotic angle. An animation of a simulation of the experiment using beam-propagation methods is available on-line in the supplementary material.

In order to tackle this problem mathematically, we perform an asymptotic analysis of the integral (4) using the stationary-phase approximation. Careful inspection of the exponential's argument yields 16 such stationary points, however, to determine the asymptotic angle we need only to focus in the limit $x\to+\infty$, $y\to-\infty$, where the astigmatic Airy's tail is evident and the angle v is measured. Under these conditions, it may be shown that only two stationary points contribute to the integral. Furthermore, due to the super-exponential decay of the Airy function in the positive $+x\to\infty$ direction, the asymptotic approximation up to terms of order $\sim a$ may be concluded to be

$$\begin{aligned}F\left(k_\xi,k_\eta,\beta,a\right)&\approx\frac{\pi\beta^{3/2}}{\left(-k_\xi k_\eta\right)^{1/4}}\\ &\times\exp\left(-\frac{2}{3}\beta^{3/2}k_\xi^{3/2}+2a\beta^3\sqrt{-k_\xi k_\eta}-\frac{2}{3}i\beta^{3/2}k_\eta\sqrt{-k_\eta}-\frac{i\pi}{4}\right).\end{aligned} \tag{8}$$

Now, to determine the asymptotic angle from this expression, we need only to differentiate the real part of the exponential's argument and find the slope. This finally yields the main result,

$$v(\beta)=\frac{\pi}{4}+\mathrm{atan}\left(\frac{1}{-1+(q\beta)^{-3/2}}\right) \tag{9}$$

where q is a fitting parameter dependent, in experiment, on the preset parameters of the optics system. The validity condition for these approximations is $(q\beta)^3\ll 1$, and we note that in this elliptic system, $v\in(\pi/4,\pi/2)$. A detailed derivation is available in the supplementary material.

So far we have found a relationship between β, which solely defines the mask in the fabrication, to the asymptotic angle v measurable in experiment. We recall that in the TEM, the diffraction plane is imaged to the CCD camera plane with magnification M, so it may finally be observed. In the experiment, we maintain a collimated input beam so the diffraction plane coincides with the focal length f of the system. It is important to understand that due to the nonlinear trajectory of the Airy beam, the magnification factor M affects the longitudinal and transverse length scales differently, effectively reducing the observed acceleration, $\mathfrak{a}_{cam}$, by a factor of M relative to the intrinsic acceleration $\mathfrak{a}$, so $\mathfrak{a}_{cam}=\mathfrak{a}/M$ (see supplementary).

Utilizing the theoretical background developed here and backed by numerical simulations, we measured the asymptotic angles of 10 Airy beams with different nodal trajectories, some of which are depicted in Fig. 2. The same Au coated SiN membrane as in the case of the vortex masks was used, where Airy binary gratings (Fig.2c) were fabricated with

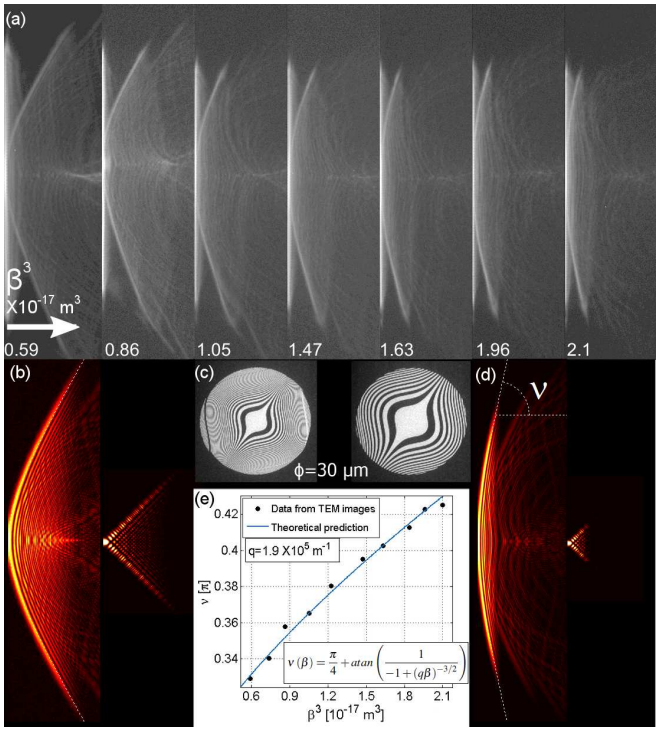

Figure 2: (Color online) Astigmatic Airy beams. (a) selected measurements; (b) simulated Airy beams (right) and their corresponding astigmatic transform (left); (c) on-axis binary masks recorded in TEM of the lowest and highest acceleration; (d) same as (b), for higher acceleration; (e) acceleration dependence of the hyperbola's asymptotic angle v according to the asymptotic model.

varying β^3 values in the range $\left(5.9 \leq \beta^3 \leq 21\right) \times 10^{-17}\mathrm{m}^3$, which for our setup corresponded to accelerations in the range $\left(1.2 \leq \mathfrak{a}_{\mathrm{cam}} \leq 4.1\right) \mu\mathrm{m}^{-1}$, assuming $f = 10\,\mathrm{cm}$ and measuring the magnification, $M = 1015$, directly using a Bragg diffraction grating of $400nm$ period. The Airy gratings impose a cubic phase modulation, due to Eq.(6), on the beam, yielding an Airy pattern in the diffraction plane (Fig.2b,d). Upon enforcing elliptical astigmatism using the TEM's stigmator lenses, the Airy beams were transformed into curved shapes, whose envelopes were well represented by hyperbolae (experimentally in Fig.2a, also in simulation in 2b,d). In order to achieve the largest angles in the vicinity of $\pi/2$, we harnessed both the condenser and objective stigmators, carefully aligning them to act in the same direction. Deviations from a symmetric hyperbola may be attributed to small misalignment of the stigmators. During the fitting process, the hyperbolic amplitude b was taken as constant; if a higher range of accelerations is desired, then the variation of b may have to be taken into account. The effect of changing the measure of ellipticity (a), which is a constituent of q and controlled by the stigmators, may prove useful in selection of a different working point on the curve $v\left(\beta\right)$, thus shifting or expanding the range of angles. q for given system conditions may be determined by a calibration sample. Thus, as evident from the fit of the experimental results to Eq.(9), shown in Fig.2e, we provide a method to finding the the nodal trajectory, or acceleration coefficient, β, from measurements of the asymptotic angle.

In this letter we examined a method of measuring the OAM of electron vortex beams by means of elliptical transformation, previously employed in light-optics using cylindrical lenses. The transformation is applied literally by the turn of a knob in any standard TEM by correctly manipulating the lens stigmators. Since OAM can be transferred between the electron beam and the internal electron states in an atom, this method can be readily applied for microscopic studies of materials [22] in electron microscopy, assuming pure-states emerge; a different approach must be taken otherwise. We extended the scope of this transformation and applied it to Airy beams in numerical simulation, beam-propagation simulation and experiment, and found an analytic, asymptotic approximation relation between the curvature of the resulting astigmatic shape and the Airy beam's acceleration, or nodal trajectory. Our results warrant further theoretical investigation into the astigmatic transform of other beams to which it may be relevant, such as Bessel beams [23], parabolic beams [24] and beams with arbitrary caustic curves [25, 26], unveiling their underlying propagation parameters.

The authors would like to acknowledge Dr. Yigal Lilach for his support in the fabrication process. The work was supported by the Israel Science Foundation, grant no. 1310/13, and the Australian Research Council.

* Electronic address: royshilo@post.tau.ac.il

[1] J. Verbeeck, H. Tian, and P. Schattschneider, Nature **467**, 301 (2010), ISSN 1476-4687, URL http://www.ncbi.nlm.nih.gov/pubmed/20844532.

[2] B. J. McMorran, A. Agrawal, I. M. Anderson, A. A. Herzing, H. J. Lezec, J. J. McClelland, and J. Unguris, Science (New York, N.Y.) **331**, 192 (2011), ISSN 1095-9203, URL http://www.ncbi.nlm.nih.gov/pubmed/21233382.

[3] M. Uchida and A. Tonomura, Nature **464**, 737 (2010), ISSN 1476-4687, URL http://www.ncbi.nlm.nih.gov/pubmed/20360737.

[4] L. Allen, M. W. Beijersbergen, R. J. C. Spreeuw, and J. P. Woerdman, Physical review. A **45**, 8185 (1992), ISSN 1050-2947, URL http://www.ncbi.nlm.nih.gov/pubmed/9906912.

[5] N. Voloch-Bloch, Y. Lereah, Y. Lilach, A. Gover, and A. Arie, Nature **494**, 331 (2013), ISSN 1476-4687, URL http://www.ncbi.nlm.nih.gov/pubmed/23426323.

[6] K. Saitoh, Y. Hasegawa, K. Hirakawa, N. Tanaka, and M. Uchida, Physical Review Letters **111**, 074801 (2013), ISSN 0031-9007, URL http://link.aps.org/doi/10.1103/PhysRevLett.111.074801.

[7] E. Abramochkin and V. Volostnikov, Optics Communications **83**, 123 (1991), ISSN 00304018, URL http://linkinghub.elsevier.com/retrieve/pii/003040189190534

[8] G. Machavariani, A. A. Ishaaya, L. Shimshi, N. Davidson, A. A. Friesem, and E. Hasman, Applied optics **43**, 2561 (2004), ISSN 0003-6935, URL http://www.ncbi.nlm.nih.gov/pubmed/15119626.

[9] T. Ellenbogen, I. Dolev, and A. Arie, Optics letters **33**, 1207 (2008), ISSN 0146-9592, URL

http://www.ncbi.nlm.nih.gov/pubmed/18516175.

[10] N. V. Bloch, K. Shemer, A. Shapira, R. Shiloh, I. Juwiler, and A. Arie, Physical Review Letters **108**, 233902 (2012), ISSN 0031-9007, URL http://link.aps.org/doi/10.1103/PhysRevLett.108.233902.

[11] P. Schattschneider, M. Stöger-Pollach, and J. Verbeeck, Physical Review Letters **109**, 084801 (2012), ISSN 0031-9007, URL http://link.aps.org/doi/10.1103/PhysRevLett.109.084801.

[12] V. G. Shvedov, C. Hnatovsky, W. Krolikowski, and A. V. Rode, Optics letters **35**, 2660 (2010), ISSN 1539-4794, URL http://www.ncbi.nlm.nih.gov/pubmed/20680091.

[13] V. Denisenko, V. Shvedov, A. S. Desyatnikov, D. N. Neshev, W. Krolikowski, A. Volyar, M. Soskin, and Y. S. Kivshar, Optics express **17**, 23374 (2009), ISSN 1094-4087, URL http://www.ncbi.nlm.nih.gov/pubmed/20052044.

[14] G. Guzzinati, L. Clark, and B. Armand, pp. 1–5 (2014), arXiv:1401.7211v1.

[15] A. Mair, A. Vaziri, G. Weihs, and A. Zeilinger, Nature **412**, 313 (2001), ISSN 0028-0836, URL http://www.ncbi.nlm.nih.gov/pubmed/11460157.

[16] M. P. J. Lavery, G. C. G. Berkhout, J. Courtial, and M. J. Padgett, Journal of Optics **13**, 64006 (2011), ISSN 2040-8978, URL http://stacks.iop.org/2040-8986/13/i=6/a=064006?key=crossref.8036fbba31e401b13caaee6f8138132b.

[17] C. Schulze, A. Dudley, D. Flamm, M. Duparré, and A. Forbes, New Journal of Physics **15**, 73025 (2013), ISSN 1367-2630, URL http://stacks.iop.org/1367-2630/15/i=7/a=073025?key=crossref.b5991d981c7281b2f72a01e0182a5f.

[18] M. Mirhosseini, M. Malik, Z. Shi, and R. W. Boyd, Nature communications **4**, 2781 (2013), ISSN 2041-1723, URL http://www.ncbi.nlm.nih.gov/pubmed/24216691.

[19] L. Reimer and H. Kohl, *Transmission electron microscopy - physics of image formation* (5th edition, Springer, 2008), ISBN 9780387400938.

[20] M. V. Berry, American Journal of Physics **47**, 264 (1979), ISSN 00029505, URL http://link.aip.org/link/?AJP/47/264/1&Agg=doi.

[21] G. A. Siviloglou and D. N. Christodoulides, Opt. Lett. **32**, 979 (2007).

[22] S. Lloyd, M. Babiker, and J. Yuan, Physical Review Letters **108**, 074802 (2012), ISSN 0031-9007, URL http://link.aps.org/doi/10.1103/PhysRevLett.108.074802.

[23] V. Grillo, E. Karimi, G. C. Gazzadi, S. Frabboni, M. R. Dennis, and R. W. Boyd, Physical Review X **4**, 011013 (2014), ISSN 2160-3308, URL http://link.aps.org/doi/10.1103/PhysRevX.4.011013.

[24] M. A. Bandres, Optics letters **33**, 1678 (2008), ISSN 0146-9592, URL http://www.ncbi.nlm.nih.gov/pubmed/19516358.

[25] E. Greenfield, M. Segev, W. Walasik, and O. Raz, Physical Review Letters **106**, 213902 (2011), ISSN 0031-9007, URL http://link.aps.org/doi/10.1103/PhysRevLett.106.213902.

[26] L. Froehly, F. Courvoisier, A. Mathis, M. Jacquot, L. Furfaro, R. Giust, P. A. Lacourt, and J. M. Dudley, Optics express **19**, 16455 (2011), ISSN 1094-4087, URL http://www.ncbi.nlm.nih.gov/pubmed/21935010.

[27] atan2(y,x) returns the angle in the interval $[-\pi,\pi]$ as opposed to standard $\arctan(y/x)$ which only returns angles in two quadrants in the positive x half-space.

arXiv:1402.3133v1 [physics.acc-ph] 13 Feb 2014

Supplementary Material - Unveiling the orbital angular momentum and acceleration of electron beams

Roy Shiloh,[1,*] Yuval Tsur,[1] Yossi Lereah,[1] Boris A. Malomed,[1] Vladlen Shvedov,[2] Cyril Hnatovsky,[2] Wieslaw Krolikowski,[2] and Ady Arie[1]

[1]*Department of Physical Electronics, Fleischman Faculty of Engineering, Tel Aviv University, Tel Aviv 6997801, Israel*
[2]*Laser Physics Centre, The Australian National University, Canberra ACT 0200, Australia*

I. MEASUREMENTS OF OAM OF $10\hbar$

We repeated the experiment for a charge 10 vortex beam, generated by a fork grating with a $0.5\,\mu$m carrier period: as seen in Fig. 1. A numerical beam-propagation simulation (Fig. 1c) shows similar results, where 10 dark stripes may be counted in the first order in both simulation and experiment. The second order counts 20 stripes, however, it is harder to distinguish between them due to technical limits of the CCD and stability of the TEM. It is also worth mentioning that, if the astigmatic transformation is not completely elliptic, higher orders will only be partially converted. This may be observed in the dark patch overlaying the second order in the experiment (Fig. 1b), while the "braided" dark fringes are a result of overlap of the next high-order mode. We can therefore conclude that the elliptic coordinate transformation method enables to measure vortex beam with an OAM of at least $10\hbar$.

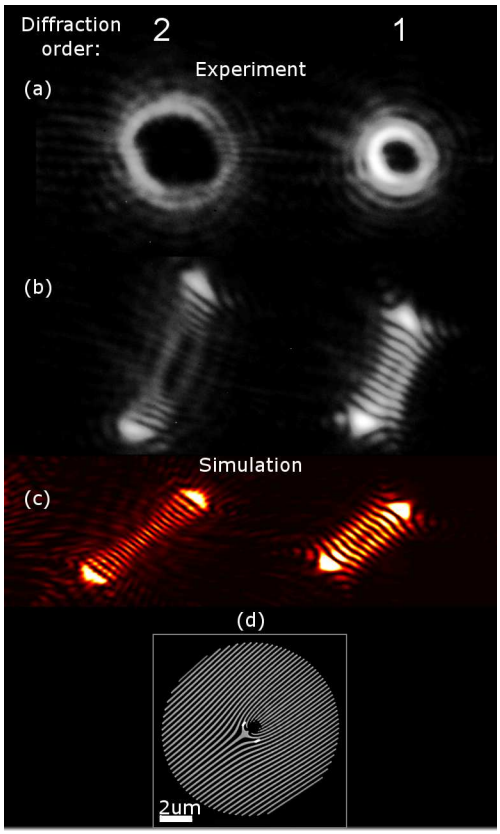

Figure 1: (Color online) Experimental results, showing two diffraction orders in focus: (a) vortices generated by a charge 10 fork grating, using a focused stigmatic beam; (b) corresponding vortices after elliptic transformation; (c) Simulation results. (d) TEM images of the charge 10 fork ($0.5\,\mu$m period). The two bright spots near the center of the fork are fabrication errors.

II. NUMERICAL INSPECTION OF THE ASTIGMATIC AIRY INTEGRAL

We numerically evaluate the two-dimensional integral,

$$F(x,y,\beta,a)=\int_{-\infty}^{\infty}\int_{-\infty}^{\infty}\exp\left[i\phi(\xi,\eta)\right]d\xi d\eta \tag{1}$$

with the phase

$$\phi(\xi,\eta)=x\xi+y\eta+2a\xi\eta+\left(3\beta^3\right)^{-1}\left(\xi^3+\eta^3\right). \tag{2}$$

In the Letter, we use the notation $k_\xi \equiv x$ and $k_\eta \equiv y$ to signify that the result is in the diffraction plane. Here we use x,y for elegance of the mathematical derivation.

It is physically acceptable to interpret β as the parameter defining the nodal trajectory curve of the Airy beam. The parameter a is a measure of the efficacy of the elliptic transformation. For the two example cases depicted in Fig.2, we see that for the stigmatic Airy ($a=0$, Fig.2a,b), the asymptotic angle υ equals 0, measured from the negative y-axis to a vertical line well-defined by the Airy lobes, regardless of β. For the astigmatic Airy ($a=1$, Fig.2c,d), β affects the result of the integral by changing the asymptotic angle υ: as the parameter β increases, so does the angle υ, measured from from the negative y-axis to the asymptotic tail of the transformed two-dimensional Airy pattern (see Fig.2d). To recover the asymptotic angle analytically, we must focus on the region $+x>0$, $-y>0$, and specifically $+x\to\infty$, $-y\to\infty$.

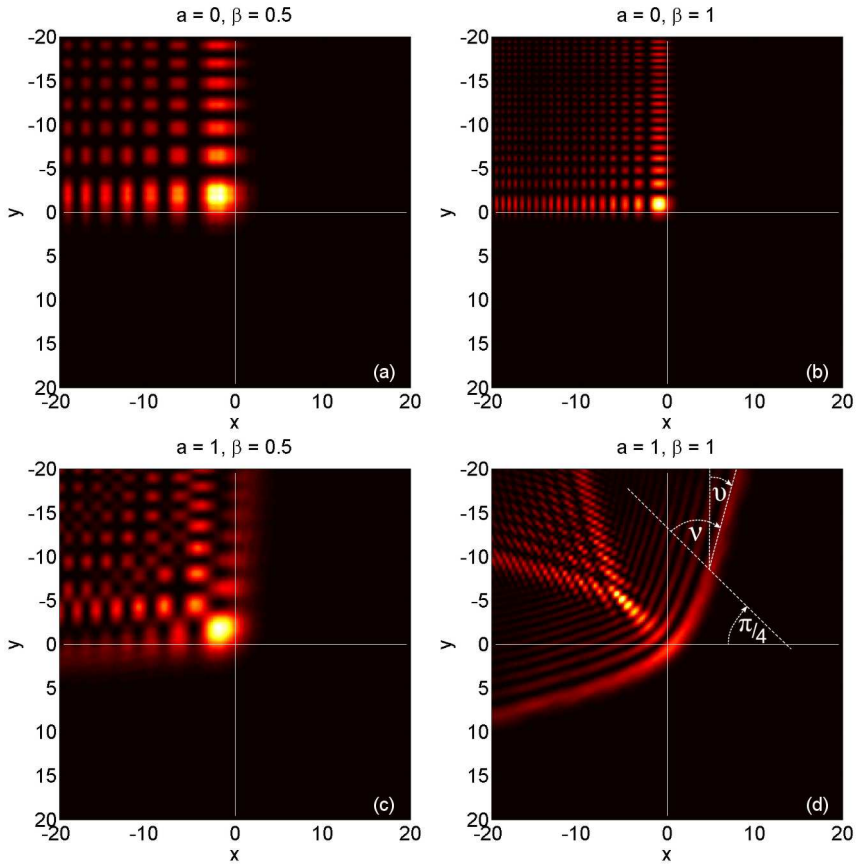

Figure 2: Numerical evaluation of expression (1): (a,b) stigmatic ($a=0$) Airy and (c,d) astigmatic ($a=1$) Airy for $\beta=0.5,1$. Definitions of the angles are depicted in (d).

III. ASYMPTOTIC APPROXIMATION OF THE ASTIGMATIC AIRY INTEGRAL

Here we solve the integral (1) by asymptotic means. We first note an obvious symmetry,

$$F(x,y,\beta,a)=F^*(x,y,\beta,-a) \tag{3}$$

where $*$ stands for the complex conjugate. Thus, F is purely real only at $a=0$. It is also noted that for $a=0$ the result of the integral is proportional to the two-dimensional Airy function, $\mathrm{Ai}(x)\,\mathrm{Ai}(y)$.

For the asymptotic evaluation of the integral, it is necessary to find the stationary-phase point (SPP), (ξ_0,η_0), at which $\phi_\xi=\phi_\eta=0$ (the subscripts stand for partial derivatives). As follows from (2), the equations which determine the SPP are

$$\begin{aligned} x+2a\eta_0+\beta^{-3}\xi_0^2 &= 0,\\ y+2a\xi_0+\beta^{-3}\eta_0^2 &= 0. \end{aligned} \tag{4}$$

These two coupled quadratic equations in ξ_0,η_0 may be decoupled into two quartic equations yielding 16 roots, which are the SPPs. However, in the limits $+x\to\infty$, $-y\to\infty$, the expression is oscillating along y and evanescent along x; then, the SPPs may be determined by asymptotic expansion to leading order in a, yielding two relevant sets of coordinates,

$$\begin{aligned} \xi_0 &\approx i\beta^{3/2}\sqrt{x}\pm ia\beta^3\sqrt{-\frac{y}{x}},\\ \eta_0 &\approx \pm\beta^{3/2}\sqrt{-y}\mp ia\beta^3\sqrt{-\frac{x}{y}}, \end{aligned} \tag{5}$$

as indicated with the help of $\pm$. At these two SPPs, the expression for the phase, taken in the present approximation, is written

$$i\phi\left(\xi_0,\eta_0\right)\approx -\frac{2}{3}\beta^{3/2}x^{3/2}\pm\frac{2}{3}i\beta^{3/2}y\sqrt{-y}\mp 2a\beta^3\sqrt{-xy}. \tag{6}$$

The second derivatives at the SPPs are:

$$\phi_{\xi\xi}\left(\xi_0,\eta_0\right)\approx 2i\beta^{-3/2}\sqrt{x},\ \phi_{\eta\eta}\left(\xi_0,\eta_0\right)\approx\pm 2\beta^{-3/2}\sqrt{-y},\ \phi_{\xi\eta}\left(\xi_0,\eta_0\right)=2a. \tag{7}$$

Finally, the computation of the integral (1) in the asymptotic approximation yields the following result:

$$\begin{aligned} F\left(x,y,\beta,a\right) &\approx \frac{\pi\beta^{3/2}}{(-xy)^{1/4}}\exp\left(-\frac{2}{3}\beta^{3/2}x^{3/2}\right)\\ &\times\left[\exp\left(-2a\beta^3\sqrt{-xy}+\frac{2}{3}i\beta^{3/2}y\sqrt{-y}+\frac{i\pi}{4}\right)+\exp\left(2a\beta^3\sqrt{-xy}-\frac{2}{3}i\beta^{3/2}y\sqrt{-y}-\frac{i\pi}{4}\right)\right] \end{aligned} \tag{8}$$

We check this approximation at $a=0$ and note that it indeed reduces to the product of asymptotic approximations for the usual Airy functions, in which case expression (8) is also purely real.

However, at $a\neq 0$ it is complex. In fact, in the case of $a>0$ and $-xy\to\infty$, the second term in the square brackets is exponentially large in comparison to the first term, hence (8) may be reduced to the one with a single leading term,

$$F\left(x,y,\beta,a\right)\approx\frac{\pi\beta^{3/2}}{(-xy)^{1/4}}\exp\left(-\frac{2}{3}\beta^{3/2}x^{3/2}+2a\beta^3\sqrt{-xy}-\frac{2}{3}i\beta^{3/2}y\sqrt{-y}-\frac{i\pi}{4}\right). \tag{9}$$

Formally, both expressions (8) and (9) may give an exponentially large result in the case of $a^2\beta^3(-y)\gg x^2$. However, the asymptotic approximation is not valid in this case, as its validity is determined by the condition that corrections $\sim a$ in Eqs.(5) are small in comparison with the leading terms, i.e., $a^2\beta^3(-y)\ll x^2$, $a^2\beta^3 x\ll y^2$.

IV. MATHEMATICAL DERIVATION OF THE RELATION $\nu(\beta)$

In the limit $+x\to\infty$, $-y\to\infty$, the expression in Eq.9 produces linear, parallel contours with an angle to the axes. Assuming $+x,-y$ tend to infinity equally fast, i.e. $+x=-y\triangleq\tilde{q}\to\infty$, this angle is solely determined by the real part of the exponent's argument of Eq.(9),

$$\varphi\left(x,y,\beta,a\right)=-\frac{2}{3}\beta^{3/2}x^{3/2}+2a\beta^3\sqrt{-xy}, \tag{10}$$

by calculating the slope,

$$Slope = \frac{\varphi_y}{\varphi_x} = \frac{ax}{ay + x\sqrt{-y\beta^{-3}}} = \frac{1}{-1 + (q\beta)^{-3/2}} \tag{11}$$

where for elegance we define $q = \tilde{q}^{-1/3} a^{2/3}$ and $q > 0$. The angle of this slope is then given by $\upsilon = \mathrm{atan}\,(Slope)$ with respect to the negative y-axis . In the experiment, however, it is easier to determine the angle relative to the inversion symmetry of the astigmatic Airy's curve, i.e. following a -45° (clockwise) rotation of the image relative to the (still horizontal and vertical) x,y axes. In this case, we define the angle $\nu = \pi/4 + \upsilon$, measured from the negative x-axis to the asymptotic tail of the astigmatic Airy (see 2d). Since in the proposed elliptical system $\upsilon \in (0, \pi/4)$, it is now obvious that $\nu \in (\pi/4, \pi/2)$, owing to the fundamental right-angle appearance of the stigmatic Airy pattern. We therefore write the final result,

$$\nu(\beta) = \frac{\pi}{4} + atan\left(\frac{1}{-1 + (q\beta)^{-3/2}}\right) \tag{12}$$

where q is now a fitting parameter dependent, in experiment, on the stigmator lens through a and the effective scaling through $\tilde{q}$. The exact dependence may be deduced by further investigation. To finalize the discussion, recall that the asymptotic approximation is valid, under the assumptions above, for $a^2\beta^3 \ll \tilde{q}$. Not incidentally, this may be rewritten $(q\beta)^3 \ll 1$ and in given experimental conditions may be approximated further. An animation of a simulation of the experiment using beam-propagation methods is available on-line in the supplementary material.

V. DERIVATION OF THE NODAL TRAJECTORY

The integral representation of the Airy function [1] may be rewritten to yield

$$\int_{-\infty}^{\infty} \exp\left[i\left(\frac{\xi^3}{3\beta^3} + \frac{zk_{DB}}{2f^2}\xi^2 + k_\xi \xi\right)\right] d\xi = 2\pi\beta \exp\left[-\frac{iz\beta^3 k_{DB}}{2f^2}\left(k_\xi - \frac{\beta^3 k_{DB}^2}{6f^4} z^2\right)\right] \mathrm{Ai}\left[\beta\left(k_\xi - \frac{\beta^3 k_{DB}^2}{4f^4} z^2\right)\right], \tag{13}$$

where the derivation is trivially extendable to (2+1)D. Under the paraxial approximation, the length scale may be written as

$$\beta k_\xi = \beta \frac{k_{DB}}{f} x \equiv \frac{x}{x_0}. \tag{14}$$

Thus the argument of the Airy function now gives the familiar form [2],

$$\mathrm{Ai}\left[\frac{1}{x_0}\left(x - \frac{1}{4k_{DB}^2 x_0^3} z^2\right)\right] \tag{15}$$

and the nodal trajectory parameter, sometimes referred to as the acceleration parameter, is understood to be

$$\mathfrak{a} = \frac{1}{2k_{DB}^2 x_0^3}. \tag{16}$$

In the TEM, the diffraction plane is imaged to the CCD camera plane with magnification M. We may therefore define the transverse x_{cam} and on-axis z_{cam} displacements with this magnification,

$$x_{cam} = M \cdot \frac{z^2}{4k_{DB}^2 x_0^3}, \tag{17}$$

$$z_{cam} = M \cdot z. \tag{18}$$

It therefore follows that

$$x_{cam}\left(z_{cam}\right)=\frac{1}{M}\frac{z_{cam}^{2}}{4k_{DB}^{2}x_{0}^{3}} \tag{19}$$

and understood that in the camera plane, the observed parameter $\mathfrak{a}_{cam}$ obeys $\mathfrak{a}_{cam}=\mathfrak{a}/M$. Thus, we finally obtain

$$\mathfrak{a}_{cam}=\frac{\beta^{3}k_{DB}}{2Mf^{3}}. \tag{20}$$

---

* Electronic address: royshilo@post.tau.ac.il

[1] O. Vallée and M. Soares, *Airy Functions and Applications to Physics* (Imperial College Press, 2004), ISBN 1860944787, URL http://books.google.co.il/books/about/Airy_Functions_And_Applications_To_Physi.html?id=Rms5FnMuKEgC&pgis=1.

[2] N. Voloch-Bloch, Y. Lereah, Y. Lilach, A. Gover, and A. Arie, Nature **494**, 331 (2013), ISSN 1476-4687, URL http://www.ncbi.nlm.nih.gov/pubmed/23426323.